One-Dimensional Simulation of Transient Flows in Non-Newtonian Fluids

Alireza Khamoushi[1]; Alireza Keramat[2]; and Ali Majd[3]

Abstract: Despite preceding studies of transients in non-Newtonian fluids that use two-dimensional (2D) models to predict the velocity gradient required to estimate unsteady losses, this study proposes an efficient one-dimensional (1D) approach. To this aim, Zielke's solution of unsteady friction is adopted for power-law and Cross fluids. The Hagen–Poiseuille profile is assumed for variations of axial velocity at each cross section, thus allowing for the computation of the shear rate to describe the viscosity in a specific non-Newtonian fluid (e.g., using power-law). The calculated transient viscosity updates the weight function of Zielke's model at each time increment in an iterative process. To verify the proposed numerical solution, the computational results are compared with available experimental data from literature and with an alternative 2D numerical solution. The comparisons demonstrate that although the proposed method is extremely simpler for practical applications, it is efficient and provides reasonable results. **DOI: 10.1061/(ASCE)PS.1949-1204.0000454.** © *2020 American Society of Civil Engineers.*

Author keywords: Transient pipe flow; Unsteady friction; Non-Newtonian fluids; Shear-thinning fluids.

Introduction

Transient flows are often observed in both natural and engineering systems, such as blood flow in the human arterial network, power plants, and oil transportation pipelines. During a transient pipe flow, a series of positive and negative pressure waves have emerged that form as a consequence of sudden changes in boundary conditions (Brunone et al. 2000). In industrial systems, such excitations can be caused by some events such as pump start up or stoppage, valve maneuvers, and bursts. In biological systems, unsteady flows are generated by several factors such as a person's heartbeat and strokes. The transient events can sometimes produce considerable pressures with huge forces (Wylie et al. 1993). Fluids treated in the classical theory of fast transient flows are generally Newtonian fluids; however, the majority of complex fluids used in practical applications exhibit shear-thinning behavior. The unsteady flow of non-Newtonian fluids may be approached from three perspectives. The first perspective is to distinguish between laminar and turbulent flows; the second is to examine fluid behaviors during steady and unsteady flows, and the third is to determine the properties of Newtonian and non-Newtonian fluids (Irgens 2013; Chen and Barbieri 2013). Mathematical modeling of non-Newtonian flows forms a fundamental research topic in fluid mechanics.

In recent years, the simulation of non-Newtonian fluids in an unsteady state is implemented using complex two-dimensional (2D) models that calculate the velocity gradient (Wahba 2013; Tazraei and Riasi 2015; Majd et al. 2016; Azhdari et al. 2017). Unlike one-dimensional (1D) models, the 2D models require a high volume of mathematical operations and computational efforts. To simplify this deficiency, this study adopts a 1D model to approximate the velocity gradient and to estimate the unsteady friction. More specifically, the velocity profile is assumed to follow the Hagen–Poiseuille velocity profile; hence, the gradient of this velocity profile is incorporated.

Unsteady friction models are exploited for modeling the shear stress variations in the momentum relation. To this aim, the most prominent research in the field of unsteady friction for Newtonian fluids is Zielke's analytical solution for laminar flows (Zielke 1968). The Zielke complex solution, however, suffers from the need for a heavy computational process. In fact, due to the dependence of the unsteady friction term on the history of flow fluctuations, it is necessary to repeat the calculations for each time step from the beginning of the onset of transients. Therefore, numerical computations developed for the original Zielke's model are cumbersome, so their use in engineering works is limited. However, several researchers used Zielke's theoretical relations for transients in 1D flows as a reference for validating their solutions (Trikha 1975; Achard and Lespinard 1981; Kagawa et al. 1983; Brown 1984; Suzuki et al. 1991). Vardy and Brown (1995, 2004a) derived weighting functions from a uniform core approximation of shear layer in transient turbulent flow. The researchers proposed relationships for smooth-pipe turbulent flows (Vardy and Brown 1995, 1996, 2003) and rough-pipe turbulent flows (Vardy and Brown 2004a) by dividing the cross-sectional area of the pipe into different regions, but the problem is still the complexity of numerical computations of the convolution integral term and the timing of analysis, which is similar to Zielke's method. Vítkovský et al. (2006a, b) offered a quick, efficient, and accurate procedure to implement the Zielke transient friction solution. The authors approximated the original weighting functions in the convolution integrals by exponential functions allowing for favorable recursive numerical approximations to the integrals. Wahba (2006) adopted the

[1]M.Sc. Graduate, Dept. of Civil Engineering, Jundi-Shapur Univ. of Technology, P.O. Box 64615-334, Dezful, Iran. Email: alirezakhamoshi@gmail.com

[2]Assistant Professor, Dept. of Civil Engineering, Jundi-Shapur Univ. of Technology, P.O. Box 64615-334, Dezful, Iran (corresponding author). ORCID: https://orcid.org/0000-0002-6280-4931. Email: keramat.alireza@gmail.com

[3]Consultant Engineer, Technical Dept., Khuzestan Water and Power Authority, P.O. Box 61335-137, Ahvaz, Iran. Email: alimajd123@gmail.com

Note. This manuscript was submitted on April 5, 2019; approved on October 23, 2019; published online on April 2, 2020. Discussion period open until September 2, 2020; separate discussions must be submitted for individual papers. This paper is part of the ***Journal of Pipeline Systems Engineering and Practice***, © ASCE, ISSN 1949-1190.

Runge–Kutta (for time derivatives) and central difference (for spatial derivatives) scheme to simulate fast transients of 1D and 2D flows including both laminar and turbulent cases. Wahba (2006) showed his proposed method is in good agreement with analytical solutions and experimental data available from the literature.

The major contribution of Brunone et al. (1991, 1995, 2000) to the unsteady friction simulation led to a new approach for modeling transients supported by several scientists. The scheme, being more simple but efficient, adopts a spacial acceleration that accounts for the complex convolution integral.

Pezzinga (1999, 2000) proposed a quasi-2D model for transient turbulent flow of a pipe network and found better results than 1D models. In addition, Pezzinga et al. (2014) analyzed transients based on the 2D simulation in pressurized polymeric pipes modeled by Kelvin–Voigt elements. Significant differences between the transient response of viscoelastic and elastic pipes are indicated in their model. The authors showed that viscoelastic models represent a faster decay of pressure oscillations and velocity profiles because of a time-lag between pressure oscillations and retarded circumferential strain. Vardy and Brown (2010, 2011) proposed solutions for unsteady pipe flows of non-Newtonian fluids with time-dependent viscosities. The results showed that such flows can be analyzed relatively simply by the use of finite Hankel transforms, and from which, the authors have found results of favorable accuracy.

It is necessary to mention the fundamental researches on non-Newtonian pipe flow that were conducted by Metzner and Reed (1955) and Dodge and Metzner (1959) who reported the variation of friction factor with Reynolds number in laminar, transitional, and turbulent flows of shear-thinning fluids. The investigations of Pinho and Whitelaw (1990) and later Escudier et al. (1992) on turbulent flows with shear-thinning incorporating power-law indices between 0.39 and 0.90 showed significant drag force reduction. In the present work, the viscosity is described using either the power-law (Ikoku and Ramey 1978; Chhabra and Richardson 2011; Irgens 2013) or Cross (Chhabra and Richardson 2011) models. Several researchers such as Toms (1948), Holmboe and Rouleau (1967), Ikoku and Ramey (1978), and Bird et al. (1987) investigated the capability of these models via experimental and numerical studies.

Wahba (2013) studied the effects of non-Newtonian nature of unsteady flow using 2D numerical simulation. He realized that transient layers were strongly influenced by the non-Newtonian fluid behavior for both shear-thinning and shear-thickening fluids. Tazraei and Riasi (2015) worked on the laminar fast transient flow, specifically its difference between shear-thinning liquids and Newtonian liquids under similar conditions. The results showed that the non-Newtonian behavior of fluids has a significant influence on the velocity and shear stress profiles and also on the magnitude of pressure head and wall shear stress. Similarly, Majd et al. (2016) investigated the unsteady laminar flow in power-law and Cross models. They concluded that the reduction of viscosity at the pipe wall decreases the frictional forces and hence leads to a decreased line-packing effect. In addition, Azhdari et al. (2017) presented a parametric study on the laminar fast transient flow of the power-law fluids through helical pipes. The results demonstrated that the main characteristics of the unsteady flow such as pressure head response, velocity and shear stress profiles, and wall shear stress change because of the nature of Newtonian and non-Newtonian fluid during transients. Sadikin et al. (2018) recently studied the effect of temperature on non-Newtonian fluids. Focused on industrial implications, they showed that the rheological properties of such fluids significantly affect the packaging process of specific liquids. As a case study, the researchers illustrated the effect of temperature on the viscosity of chili sauce during packaging.

In the present study, a 1D solution for the transient flow of non-Newtonian fluids is proposed. Transients in shear-thinning non-Newtonian fluids, which are a sub-branch of the generalized Newtonian fluids is studied. The main characteristic of these fluids is that the isotropic viscosity of such fluids depends on flow properties (Bird et al. 1987; Chhabra and Richardson 2011; Irgens 2013). Specifically, in the current research, the viscosity is described using either the power-law or Cross models (Majd et al. 2016). The numerical solution based on the method of characteristics (MOC) is first developed and then it is adopted to simulate transients of such non-Newtonian fluids in a reservoir-pipe-valve system. The results of the proposed solution scheme are then compared with the conventional 2D solutions in terms of time histories of pressure head and velocity profiles at the midpoint of the pipe.

Mathematical Model

Transient Flow and Quasi-Steady Friction

To estimate the discharge Q and pressure head H averaged over the cross-sectional area of flow, the classical 1D water-hammer theory is adopted, which is governed by the momentum equation

$$\frac{\partial H}{\partial z} + \frac{1}{gA}\frac{\partial Q}{\partial t} + \beta = 0, \qquad \beta = \beta_s + \beta_u \tag{1}$$

and the continuity equation

$$\frac{\partial H}{\partial t} + \frac{a^2}{gA}\frac{\partial Q}{\partial z} = 0 \tag{2}$$

where t = time; z = distance along the pipe centerline; g = gravitational acceleration; D = inside pipe diameter; A = cross-sectional flow area; and a = wave speed of the fluid (Daily et al. 1956; Brunone et al. 1991, 1995; Chaudhry 2014). The frictional term (β) can be decomposed as $\beta_s + \beta_u$, where the first term (β_s) represents the contribution of viscous forces related to the quasi-steady flow condition and the other term (β_u) represents the contribution of unsteady behavior of fluid's shear stress at the pipe wall. The frictional head loss associated with quasi-steady flow conditions (β_s) is quantified according to the well-known Darcy–Weisbach equation (Travaš and Basara 2015)

$$\beta_s = \frac{\lambda}{D}\cdot\frac{V\,|V|}{2g} \tag{3}$$

in which, V = average cross-sectional velocity; and λ = Darcy–Weisbach friction factor. In the laminar flow regime, the friction factor λ is derived based on the Reynolds number ($\mathbf{R}$):

$$\lambda = \frac{64}{\mathbf{R}} \tag{4}$$

Eqs. (3) and (4) are valid for Newtonian fluids. For power-law fluids under consideration, the generalized Reynolds number ($\mathbf{R}_g$) introduced by Metzner and Reed (1955) is defined

$$\mathbf{R}_g = \frac{\rho V^{2-n} D^n}{8^{n-1} m \left(\frac{3n+1}{4n}\right)^n} \tag{5}$$

in which, m = power-law consistency coefficient; n = power-law index; and ρ = fluid density. Considering a fully developed steady-state laminar flow, the following equation between the generalized Reynolds number, friction factor λ, wall shear stress ($\tau_{w,ss}$) and average (over flow cross section) velocity V applies (Wahba 2013; Irgens 2013)

$$\lambda = \frac{2\tau_{w,ss}}{\rho V^2} = \frac{16}{\mathbf{R}_g} \tag{6}$$

Unsteady Friction in Newtonian Fluids

The unsteady friction term (β_u) based on the original version of Zielke's model (1968) comprises the convolution of a weight function (W) with transient flow accelerations $\partial V/\partial t$, as follows:

$$\beta_u = \frac{16\upsilon}{gD^2} Y(t), \qquad Y(t) = \int_0^t W(t-s)\frac{\partial V}{\partial s}(s)ds \tag{7}$$

in which, υ = kinematic viscosity. The weight function W accounts for the initial flow conditions (the Reynolds number of the flow) and the relative roughness of the pipe wall. The implementation of the original Zielke's model requires a large computer storage. Therefore, several researchers suggested remedies to resolve this drawback aiming to enhance the computational efficiency. Vardy and Hwang (1991) showed good matches between a 2D shell model of transient laminar flow and the Zielke weighting function. Ghidaoui and Mansour (2002) showed the Vardy–Brown weighting function produced good matches with the quasi-2D model of Pezzinga (1999) for smooth-pipe turbulent flow as well as with experimental data. Most importantly, Vítkovský et al. (2004) provided approximate expressions for the weighting functions of different flow regimes including laminar, smooth-pipe turbulent, and rough-pipe turbulent flow. The authors used a scaling approach; hence, their method did not require re-fitting (by minimization) for different Reynolds numbers of flow and pipe relative roughness, whereas, the Vardy and Brown (2004b) approach required re-fitting.

Non-Newtonian Fluids Definition

Non-Newtonian fluids can be divided into three general categories: time-independent fluids, time-dependent fluids, and visco-elastic fluids (Chhabra and Richardson 2011). This paper focuses on the simplest type, which falls into the time-independent fluids category, known as power-law fluids.

Power-Law Model

For a power-law fluid, the rheological equation relating the shear stress η to the shear rate dV_z/dr is similar to Newtonian fluids with this difference that the relationship between the two quantities is no longer linear and can be expressed as

$$\eta = m\left(\frac{dV_z}{dr}\right)^{n-1} = m(\dot{\gamma})^{n-1} \tag{8}$$

This definition implies that the shear stress versus an exponent of shear rate can be represented by a straight line which in reality may apply for a range of shear rates (or stresses). Considering Eq. (8), for shear-thinning fluids, $n < 1$; for shear-thickening fluids, $n > 1$; and for Newtonian fluids, $n = 1$, which then $m = \mu$, where μ represents the dynamic viscosity of the Newtonian fluid (Chhabra and Richardson 2011; Irgens 2013; Wahba 2013).

Cross Model

The Cross representation is a more advanced model with four parameters that are also more consistent with reality. The variation of viscosity η in this fluid is bounded by two specified parameters; hence

$$\frac{\eta - \eta_\infty}{\eta_0 - \eta_\infty} = \frac{1}{1 + k\dot{\gamma}^n} \tag{9}$$

In Eq. (9), n (< 1) and k are fitting parameters, whereas η_0 and η_∞ are lower and upper-bound quantities of viscosity that correspond to low and high shear rates, respectively. The Cross fluid becomes Newtonian if $k = 0$. Similarly, for $\eta \ll \eta_0$ and $\eta \gg \eta_\infty$, the model reduces to the previously defined power-law model in Eq. (8) (Chhabra and Richardson 2011).

Unsteady Friction in Non-Newtonian Fluids

The aim of this section is to derive a kinematic viscosity proportionate to the type of desired non-Newtonian fluid, based on Zielke's model. The proposed kinematic viscosity, which includes the properties of power-law or Cross fluid, is then exploited for the estimation of the existing weighting functions derived for the computation of the transient friction. This research adopts Vardy and Brown's (1995) weighting function developed based on Zielke's approach

$$W(\tau) = \frac{A^* e^{-[(\frac{4\upsilon t}{D^2 C^*})]}}{\sqrt{\frac{4\upsilon t}{D^2}}} \tag{10}$$

where t = time; $A^* = (2\sqrt{\pi})^{-1}$; and $C^* = 0.0047$ are constants in laminar flows.

Power-Law Fluid

In view of the kinematic viscosity relation ($\upsilon = \eta\rho^{-1}$) and the power-law model [Eq. (8)], the following relation governes the kinematic viscosity of the power-law fluid:

$$\upsilon = \frac{m(\frac{dV_z}{dr})^{n-1}}{\rho} = \frac{m(\dot{\gamma})^{n-1}}{\rho} \tag{11}$$

where V_z = axial (z-component) velocity; ρ = fluid density; and $\dot{\gamma}$ = Shear rate. Eq. (11) shows that to compute the viscosity, using 2D solutions is required, allowing the computation of the velocity profile in the flow cross section and hence the velocity gradient (Wahba 2013; Tazraei and Riasi 2015; He et al. 2016; Majd et al. 2016; Azhdari et al. 2017). In this research, however, the velocity profile during the transient state is assumed to be governed by the Hagen–Poiseuille velocity profile (Chhabra and Richardson 2011; Irgens 2013). In other words, the actual variations of the velocity profile and hence the viscosity are neglected, and instead, steady-state flow characteristics (Hagen–Poiseuille profile) are assumed to remain during transients. With this fundamental simplification for the velocity profile, the average cross-sectional discharge (Q) against shear stress (τ_{rz}) for power-law fluid is found to be

$$Q = \frac{\pi R^3}{\tau_w^3}\int_0^{\tau_w} \tau_{rz}^2 \left(\frac{\tau_{rz}}{m}\right)^{1/n} d\tau_{rz} \tag{12}$$

The derivation of Eq. (12) is presented in Appendix I. Further simplification of Eq. (12) yields

$$Q = \frac{\pi R^3 n}{(3n+1)m^{1/n}}\tau_w^{1/n} \tag{13}$$

According to Eq. (13) and the shear stress relation (for power-law model) at wall ($\tau_w^{1/n} = m^{1/n}\dot{\gamma}$), the following shear rate relation is obtained for power-law fluid (Khan 1992)

$$\dot{\gamma} = \left(\frac{8V}{D}\right)\left(\frac{3n+1}{4n}\right) \tag{14}$$

The coefficient $(3n+1)(4n)^{-1}$ is a correction factor that is introduced because of the power-law fluid, noting that $\dot{\gamma} = 8VD^{-1}$

for Newtonian fluids. The derived shear rate relation in Eq. (14) is substituted in Eq. (11) to determine the viscosity corresponding to the power-law fluid

$$\upsilon = \frac{m}{\rho}\left(\frac{8V}{D} \times \frac{3n+1}{4n}\right)^{n-1} \tag{15}$$

Note that the computed kinematic viscosity is treated as a transient quantity, which is updated at each time step.

Cross Fluid

The purpose of this section is to find the kinematic viscosity $\upsilon = \eta\rho^{-1}$ in terms of the mean velocity for the Cross model. The resultant kinematic viscosity is then substituted in Eq. (10) to compute the weighting function.

Assuming the Hagen–Poiseuille profile of the pipe flow (Chhabra and Richardson 2011; Irgens 2013), the following relation links the mean velocity, wall shear stress, and shear rate:

$$\dot{\gamma} = \left(\frac{8V}{D}\right)\left(\frac{3(d\ln\tau_w)(d\ln(8V/D))^{-1}+1}{4(d\ln\tau_w)(d\ln(8V/D))^{-1}}\right) \tag{16}$$

where its derivation is provided in Appendix II. For the definition of the wall shear stress (τ_w), the Cross fluid model represented in Eq. (9) is used. Accordingly, the general shear stress relationship ($\tau_w = \dot{\gamma}\eta$) considering the Cross model (given $\eta_0, \eta_\infty, k, n$) becomes

$$\tau_w = \dot{\gamma}\left(\frac{\eta_0 - \eta_\infty}{1 + k\dot{\gamma}^n} + \eta_\infty\right) \tag{17}$$

One may substitute for τ_w from Eq. (17) in Eq. (16) to arrive at a relation as a function of the shear rate. Having found the shear rate, the dynamic (absolute) viscosity η is found from Eq. (9); then, it allows for the computation of the desired kinematic viscosity and hence the weighting function.

Numerical Simulation

The major concern of transients simulation in non-Newtonian fluids is the estimation of shear stress that itself is determined by the fluid viscosity. The viscosity is essentially relevant to the variations of the cross-sectional velocity profile; hence, 2D simulations seem inevitable. However, the remarkable efforts on transforming the effects of the velocity profile (2D behavior) during water hammering to 1D quantities (Zielke 1968) and facilitating its implementation (Vardy and Brown 1995, 1996, 2003, 2004a; Vítkovský et al. 2004) can be adopted for simulating transients in non-Newtonian fluids. To this aim, the fluid viscosity is updated at each space and time step based on the mean velocity and the specific definition of the non-Newtonian property. Having found an approximate viscosity at each section, calculations at each time step proceeded by using the methods provided in the literature, but with improved viscosities. The MOC scheme and the entire iterative process are detailed in this section.

MOC Solution

In this paper, the MOC solution is used to simultaneously solve the momentum and the continuity equations. The final expressions along the positive (C^+) and negative (C^-) characteristic lines are represented respectively as follows (Chaudhry 2014):

$$C^+{:}Q_P = C_P - C_{a+}H_P \tag{18}$$

$$C^-{:}Q_P = C_N + C_{a-}H_P \tag{19}$$

where C_P, C_N, C_{a+}, and C_{a-} = coefficients evaluated through

$$C_P = \frac{Q_A + BH_A + C'_{P1} + C''_{P1}}{1 + C'_{P2} + C''_{P2}} \tag{20}$$

$$C_{a+} = \frac{B}{1 + C'_{P2} + C''_{P2}} \tag{21}$$

$$C_N = \frac{Q_B - BH_B + C'_{N1} + C''_{N1}}{1 + C'_{N2} + C''_{N2}} \tag{22}$$

$$C_{a-} = \frac{B}{1 + C'_{N2} + C''_{N2}} \tag{23}$$

The definitions of the coefficients/variables in Eqs. (20)–(23) depend on the numerical scheme used to describe the quasi-steady and the unsteady friction terms, as illustrated in Appendix III.

Numerical Simulation Algorithm

The proposed 1D solution of transients in the specified non-Newtonian fluids can be implemented through the following steps.

1. Perform a steady-state analysis to determine the initial conditions of the problem. The energy (Bernoulli) equation in conjunction with Eqs. (3)–(6) are used to estimate pressure head loss.
2. Eqs. (18)–(23) are used to calculate the pressure head and flow rate at the next time step. The coefficients of the characteristics equations are derived in Appendix III.
3. The estimated flow rate at the current time step is employed to find the transient viscosity using Eq. (15). This procedure is performing for all spatial nodes of MOC at the current time step.
4. Check the convergence of viscosity $|\upsilon_{r+1} - \upsilon_r| \cdot \upsilon_r^{-1} < 10^{-3}$, where the subscript r stands for the iteration number (or the convergence of the flow rate). If it is reached, go to step 5; otherwise, move to step 2 to iterate the procedure and improve the transient unknowns. In the latter case, given the new viscosity quantities corresponding to each node (obtained in step 3), the coefficients of characteristics Eqs. (18)–(23) are updated.
5. Proceed to the next time step $t_{n+1} = t_n + \Delta t$ and repeat the computations from step 2.

Numerical Results

Some of the main characteristics of the unsteady flow such as pressure head response, velocity, and shear stress profiles are scrutinized. The focus is placed upon the fluid hammer considering its behavior in the Newtonian and non-Newtonian fluids. After verifying the proposed numerical solution with that of the literature (Wahba 2013; Tazraei and Riasi 2015; Majd et al. 2016), the effects of the non-Newtonian fluids are investigated.

A pseudo-plastic liquid that behaves as a shear-thinning fluid is studied, as it is the most common non-Newtonian fluid in applications. The proposed 1D solution of unsteady flow in power-law fluids is implemented, and its results are presented in this section. The convergence of the numerical solution subject to different mesh sizes is first studied followed by comparison with experimental data from the literature. Finally, several figures show the effects of the non-Newtonian property of fluid on transients.

Pipe System Specification

Consider the Joukowsky formula for the transient pressure rise ($\Delta H = aV_0 g^{-1}$) that means the value of the transient pressure just after the excitation is directly related to the pressure wave speed and initial velocity (steady state). In this view, the same steady-state velocity is used for all simulations so the pressure rise of all tests is equivalent and hence the transient responses are merely investigated.

The pipe is made from copper and has an inner diameter $D = 0.025$ m, wave speed $a = 1,324$ ms^{-1}, and length $L = 36.09$ m. The operating non-Newtonian fluid is high viscosity oil with dynamic viscosity $\eta = 0.03484$ Pa · s and density $\rho = 876$ kg m^{-3}. The coefficients of the power-law model are chosen to be $\eta = \eta_0$ and $n = 0.6$. The initial viscosity of the power-law model is set to the viscosity of the corresponding Newtonian fluid; thus, for $n = 1$, the characteristics of the Newtonian fluid is achieved. With this value of the initial viscosity, the computational results of Newtonian fluid can readily be compared with those of non-Newtonian. Besides, the flow characteristics, which result from the nonlinear fluid property, can be identified. The Reynolds number for this laminar flow case is 82, and the fluid transient is generated by the sudden closure of the downstream valve (Fig. 1).

Verification of the Computational Solution

The computational results are examined subject to three concerns. First, the sensitivity of the results with respect to the adopted mesh size is assessed. Then, the calculated pressures heads are compared with some laboratory data available from the literature. Lastly, the results of the proposed 1D model are compared with those of the 2D model presented by Majd et al. (2016).

Convergence

Any numerical result should be tested against sensitivity to the mesh size it uses. This property of a valid numerical scheme is shown in Fig. 2, in which the variations of pressure head versus different mesh sizes are examined. The computed pressure heads correspond to the valve location and time $t = 0.1117$ (s) and belong to the Newtonian ($n = 1$) and power-law fluid with $n = 0.6$, 0.8. The results, for a relatively small mesh size, converge to a true quantity, and after which, no significant change is observed in the computations.

Comparison with Experimental Data

A laboratory transients test on the pipe system with the details stated in the pipe system specifications section was performed at Research and Advanced Development Avco Corporation by Holmboe and Rouleau (1967). The results presented in this experiment were later used by several researchers to validate their proposed mathematical or numerical solution (Wahba 2013; Tazraei and Riasi 2015; Majd et al. 2016).

The experiment results illustrate time histories of pressure heads at the valve and pipe midpoint for the Newtonian fluid case ($n = 1$). Figs. 3 and 4 compare the nondimensional experimental data (Holmboe and Rouleau 1967) with the results of the implemented numerical solution at the valve and pipe midpoint, respectively. The comparison demonstrates that the agreement between experimental and numerical results is acceptable. The slight discrepancy reported by other researchers (Wahba 2013; Tazraei and Riasi 2015; Majd et al. 2016) can be due to experimental issues or uncertainties associated with the input data to the transient model.

Comparison with the 2D Model

For the sake of verifying the proposed numerical solution scheme, the 1D results are here compared with the 2D solutions known to be

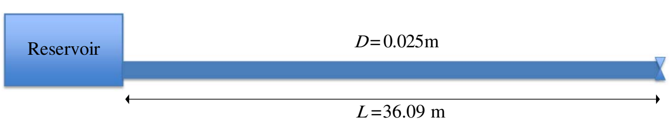

Fig. 1. Reservoir-pipe-valve system to run fluid transients tests.

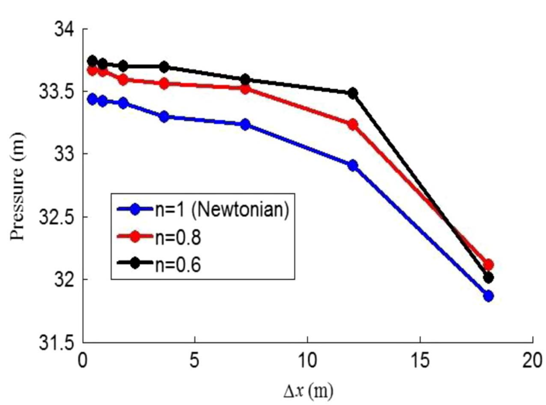

Fig. 2. Convergence of pressure head at valve location and time section $a.t.L^{-1} = 4.1$ ($t = 0.1117$) versus different computational mesh sizes.

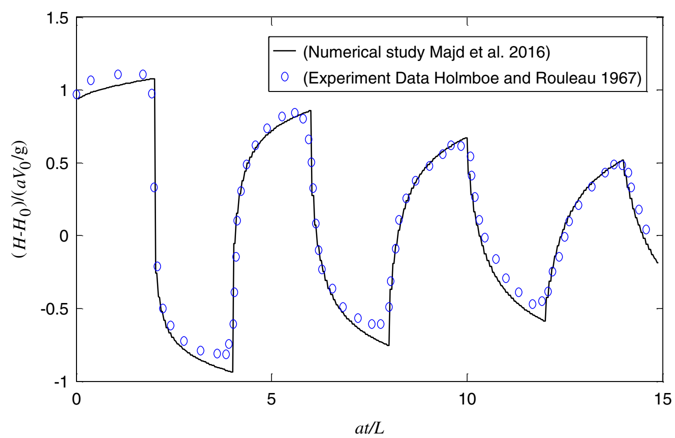

Fig. 3. Pressure time-history at the valve.

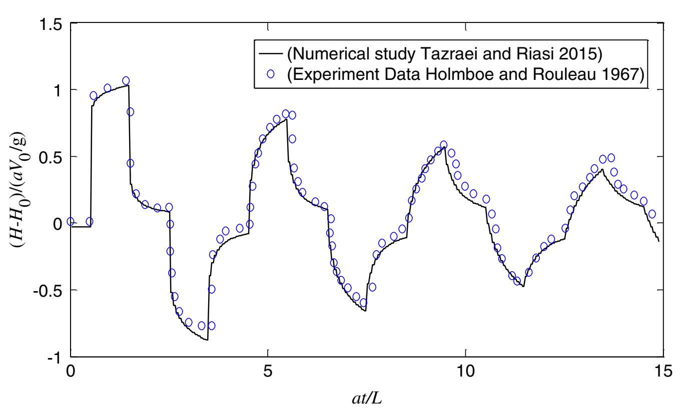

Fig. 4. Pressure time-history at the midpoint of the pipeline.

more accurate and acceptable (but harder to implement) (Wahba 2013; Tazraei and Riasi 2015; Majd et al. 2016). The input data, boundary and initial conditions of both methods share identical quantities so the results can be fairly compared. Specifically, with using equivalent initial conditions, both methods arrive at identical immediate pressure rise (Joukowsky's pressure head) which then allows for the assessment of non-Newtonian effects during transients. Fig. 5 presents the velocity profile at the steady state (initial condition) the two methods employ for different power-law coefficients. The results show that the proposed method computes the average velocity based on this velocity profile to make use of the developed formulations. During the transient phenomenon, the 2D methods use various patterns for the velocity profile dictated by the momentum equation in the radial direction (Wahba 2013; Majd et al. 2016), whereas the proposed 1D method adopts a velocity profile proportional to the one presented in Fig. 5. The computed pressure heads of the two methods are provided for the valve node (Fig. 6) and midpoint (Fig. 7). The results show that the estimated pressure heads of the proposed method are relatively close to those of the 2D method (Majd et al. 2016), so the effect of the approximate computation of viscosity and shear stress on the fluid pressure is small. These results imply that despite the simplicity of the proposed method, this method can provide satisfactory results.

As illustrated in Figs. 6 and 7, in the non-Newtonian fluid flows, the maximum pressure slightly reduces by decreasing the fluid viscosity. Likewise, the rise of the line-packing effect due to the increased shear-thinning property is observed in the results of the new method, which is consistent with the literature. In contrast, decreasing the viscosity of the fluid reduces the amount of pressure drop across the pipe path, thus declining the line-packing effect.

To quantify the error between the two solutions, the following metric is defined:

$$\mathrm{error}(t) = \left(\frac{h^{2D}(t) - h^{1D}(t)}{\mathrm{Max}(\mathbf{h}^{2D} - H_0\mathbf{1})}\right) \times 100 \tag{24}$$

in which the subscripts 1D and 2D = present and Majd et al.'s (2016) solution, respectively; H_0 = steady-state pressure head;

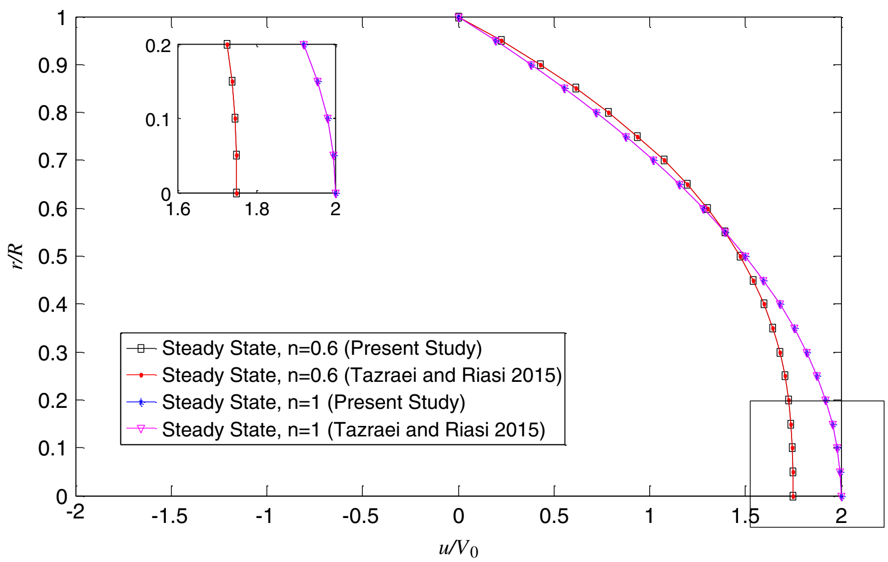

Fig. 5. Axial velocity profiles at the midpoint of pipeline in steady-state flow.

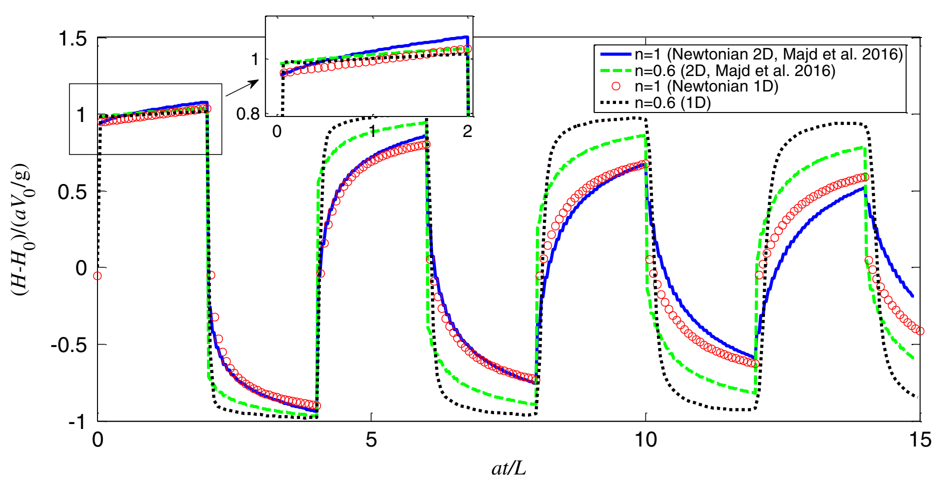

Fig. 6. Pressure time-history at the valve for different power-law fluids.

J. Pipeline Syst. Eng. Pract., 2020, 11(3): 04020019

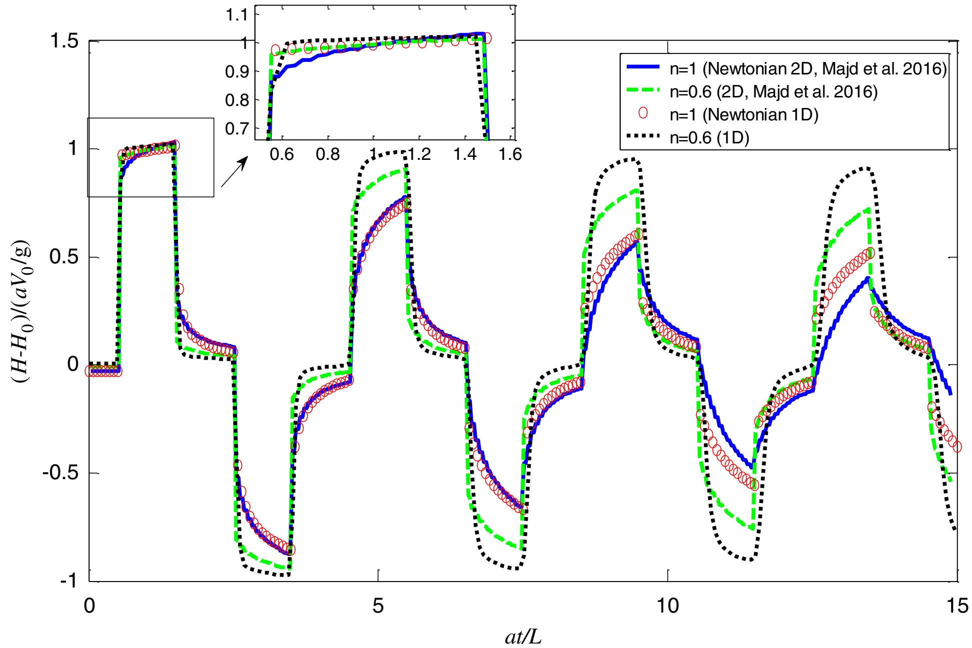

Fig. 7. Pressure time-history at the midpoint of the pipeline for various power-law fluids.

1 = column vector whose all elements are unity. The evaluated error [using Eq. (24)] between the two sets of results are shown in Fig. 8. The error quantities reveal that the difference between the two methods is noticed only at the points of sharp pressure change that essentially results from slight timing mismatch between the two computational methods. However, the results show that the proposed method can favorably capture the non-Newtonian effects, and overall, the method is reasonable for practical applications.

A similar comparison between the two methods is performed in terms of the average cross-sectional velocity versus time at the reservoir (Fig. 9) and midpoint (Fig. 10). The error estimation presented in Fig. 11 shows the evaluated discrepancy of the average velocity for the two methods. The results confirm that for the Newtonian case ($n = 1$), the 1D approach is satisfactory, which agrees with the literature. As the shear-thinning effect increases, the discrepancy starts to rise such that for $n = 0.6$, the highest mismatching is observed. Although the computed velocities are slightly overestimated, the timing of their variations demonstrates reasonable agreement.

Variations of the Velocity Profiles during Transients in the Non-Newtonian Fluid

The main reason for the discrepancy between the 1D and 2D pressure results is the approximate estimation of cross-sectional velocity profiles in the 1D scheme. To better illustrate this point, the variations of the axial velocity along the radial direction (continuous line) computed based on the 2D simulation (Majd et al. 2016) and the corresponding mean velocity (dashed) and mean velocity of the 1D solution (dotted) are compared in Figs. 12(a–f) for Newtonian and Figs. 13(a–f) for power-law fluid with $n = 0.6$. The figures display the velocities at the midpoint of the pipeline for $t = 0$ (a), $t = L/a$ (b), $t = 2L/a$ (c), $t = 3L/a$ (d), $t = 4L/a$ (e), and $t = 5L/a$ (f).

Note that the proposed 1D simulation adopts the Hagen–Poiseuille velocity profile, clearly differing from the velocity profiles of the 2D models (Martins et al. 2018; Majd et al. 2016). However, the effects of the 2D behavior can be treated via the Zielke formula, which is the basis of this 1D research (similar to what has been performed for unsteady friction). Furthermore, the gradient of the velocity profile is the main concern. More specifically, the dynamic viscosity (the fundamental variable) is estimated from the

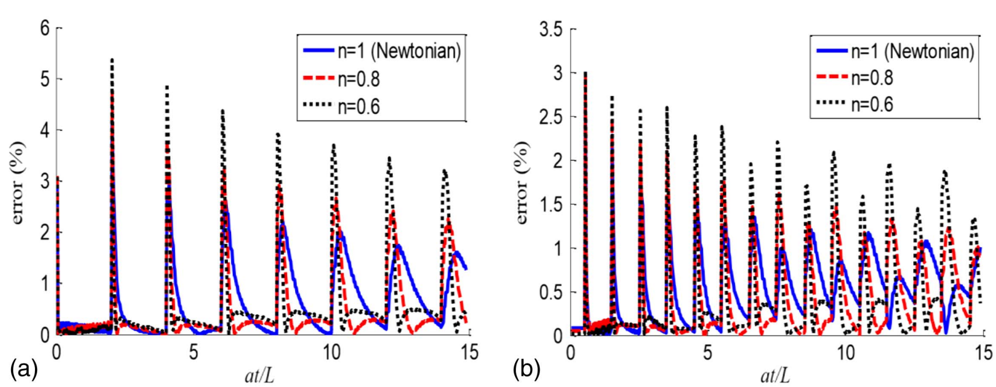

Fig. 8. Error of the computed pressure head between the present study: (a) the 2D solution of Majd et al. (2016) at the valve location; and (b) at the midpoint of the pipeline.

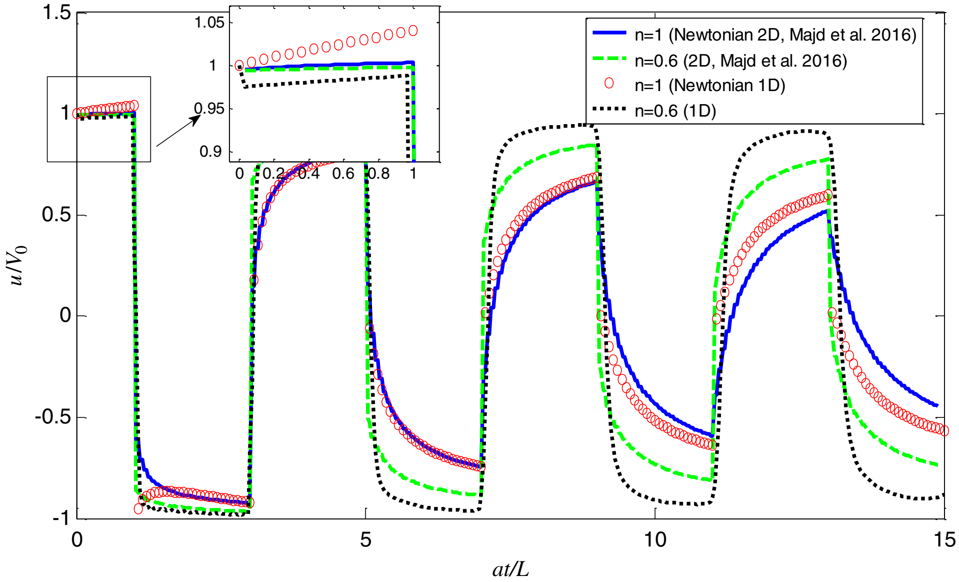

Fig. 9. History of the average velocity at the reservoir point (power-law).

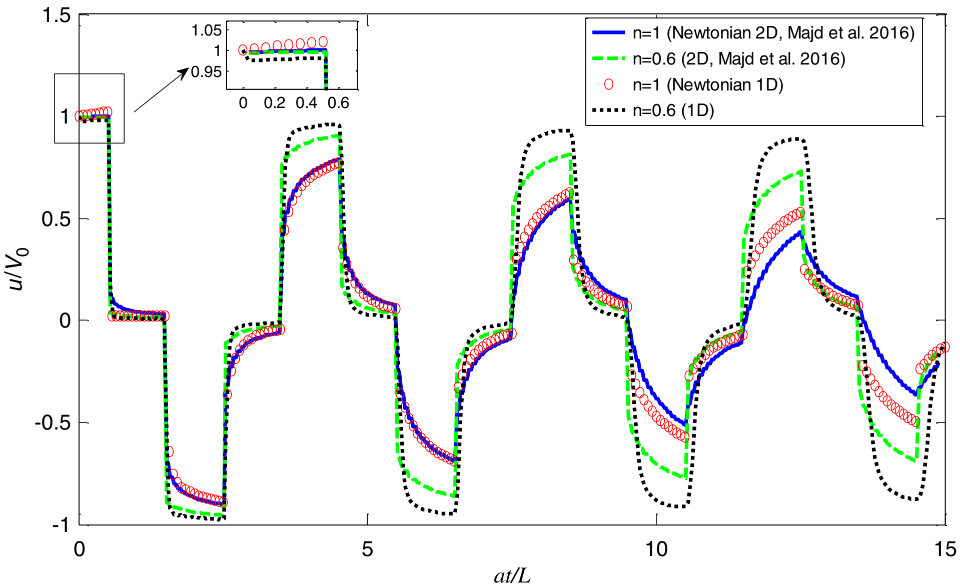

Fig. 10. History of average velocity at the midpoint of the pipeline (power-law).

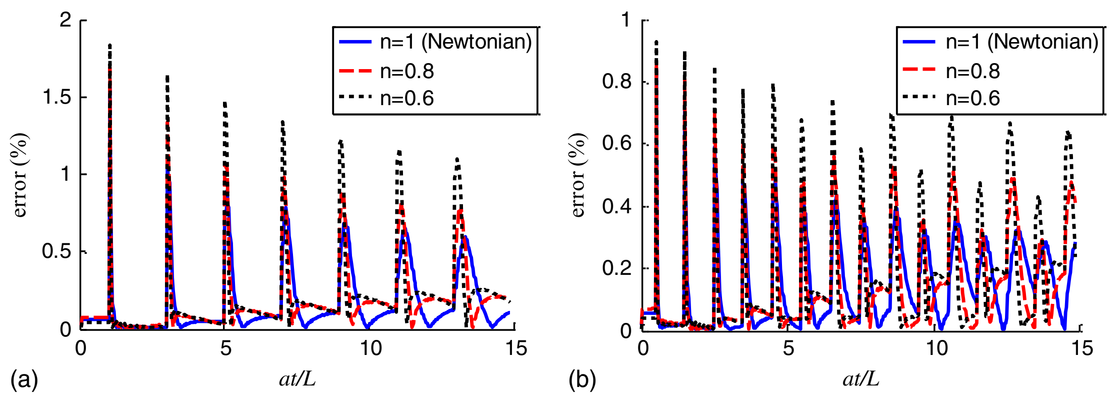

Fig. 11. Error of the computed velocity between the present study: (a) the 2D solution of Majd et al. (2016) at the valve location; and (b) at the midpoint of the pipeline.

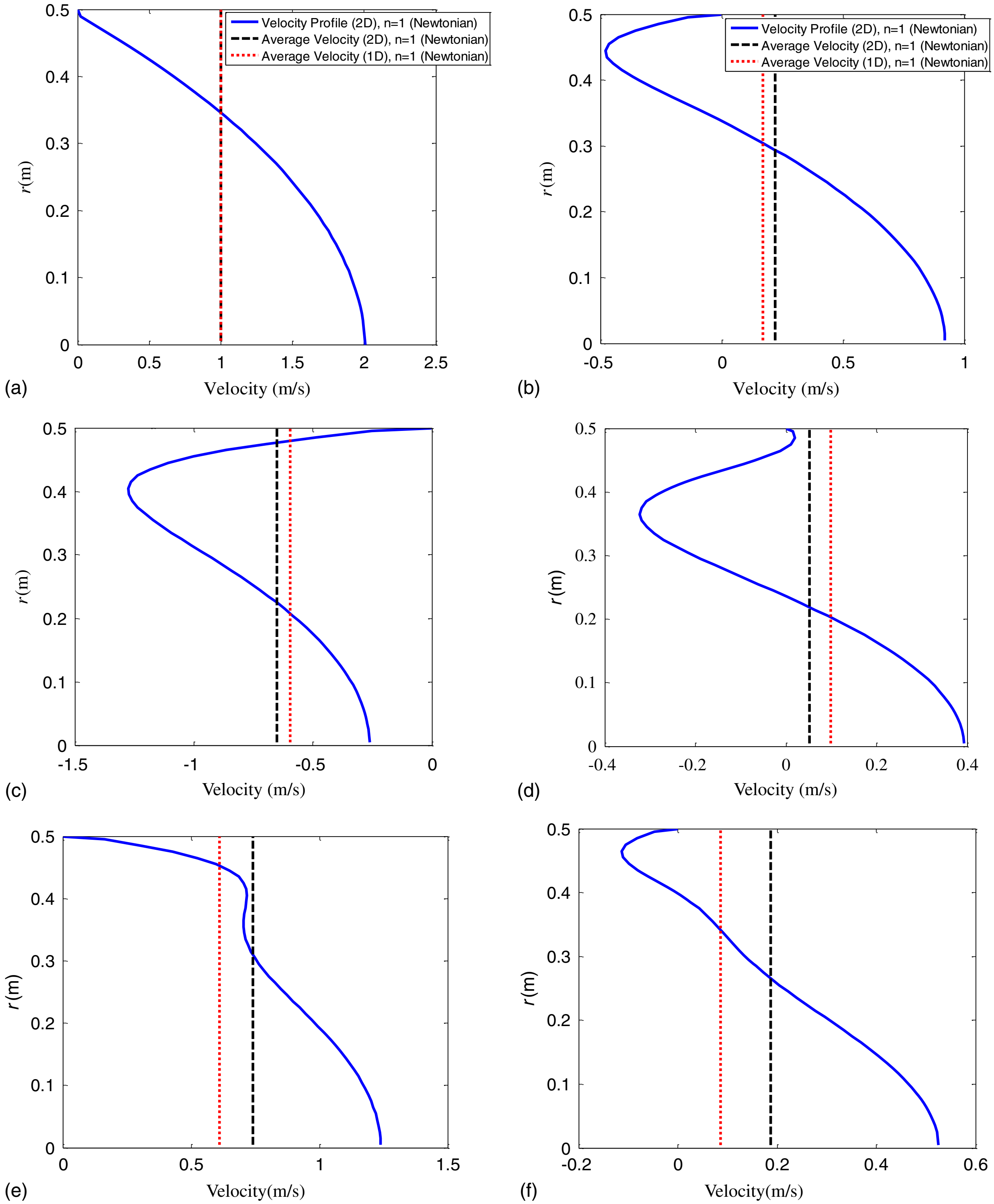

Fig. 12. Velocity profiles versus mean velocities of the 2D model (dashed) and those of the current model (dotted) at the pipe midpoint for $n = 1$ (Newtonian): (a) $t = 0$ (steady state); (b) $t = 1L/a$; (c) $t = 2L/a$; (d) $t = 3L/a$; (e) $t = 4L/\mathrm{a}$; and (f) $t = 5L/a$.

gradient of Hagen–Poiseuille profile whose computation is based on the mean velocity, which itself depends on the dynamic viscosity. Thus, the dynamic viscosity and the gradient of the velocity profile (near the wall) are updated via the explained iterative process.

Variations of the Dynamic Viscosity and Shear Stress

Some additional results are provided in this section to conceive the significance of shear-thinning fluids in the wake of transient events. In Newtonian fluids, the solution adopts a constant viscosity to be used in Eq. (10), and based on which, the weight functions are computed, then leading to the computation of velocity and pressure head at the new time step. However, herein, the viscosity depends on the mean velocity [Eq. (15)], which itself depends on the viscosity due to Eq. (9). The proposed method therefore needs to solve the nonlinear equations (e.g., by repetition between equations) to converge to a viscosity, and hence, flow rate and pressure head.

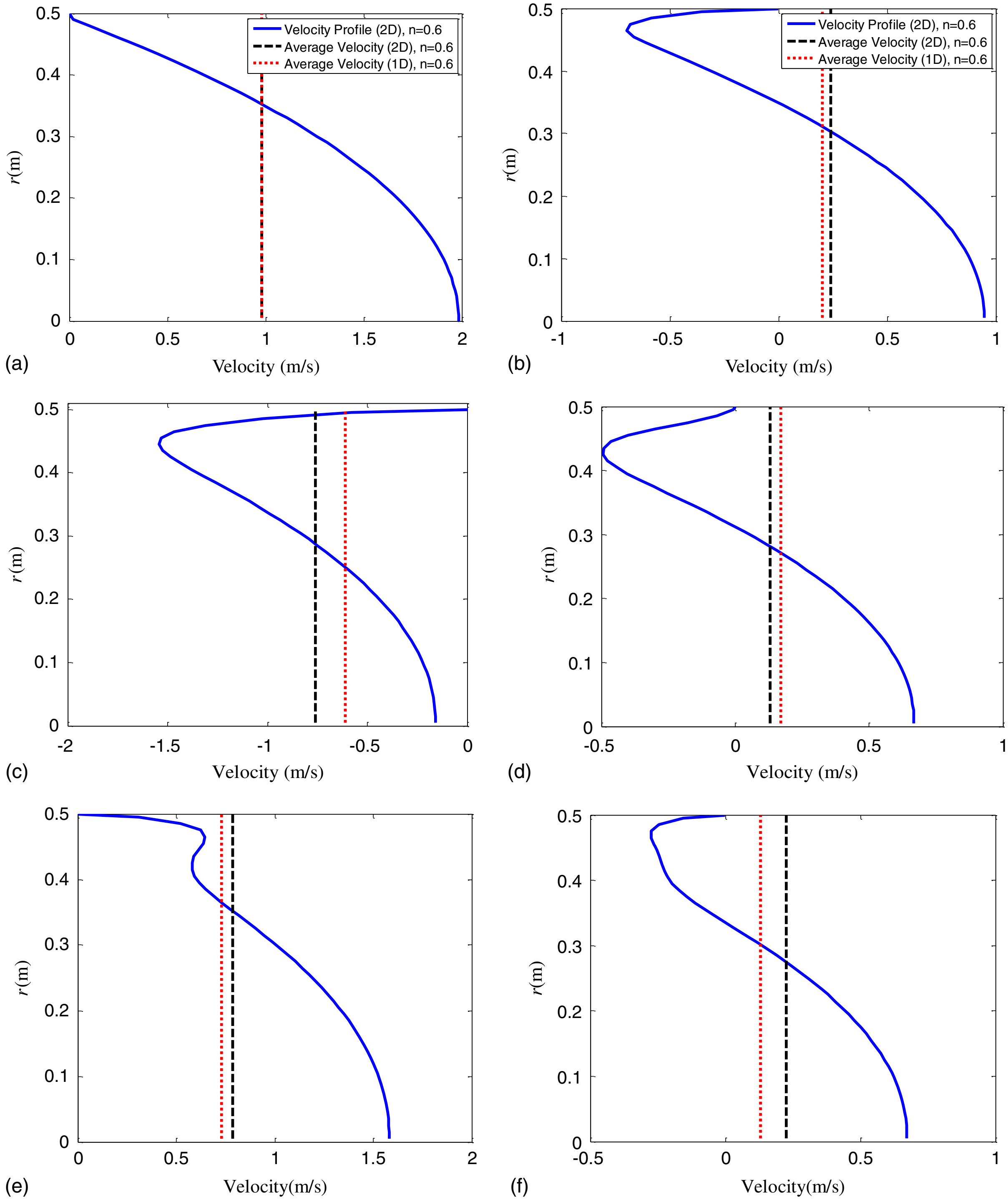

Fig. 13. Velocity profiles versus mean velocities of the 2D model (dashed) and those of the current model (dotted) at the pipe midpoint for $n = 0.6$: (a) $t = 0$ (steady state); (b) $t = 1L/a$; (c) $t = 2L/a$; (d) $t = 3L/a$; (e) $t = 4L/a$; and (f) $t = 5L/a$.

Fig. 14 illustrates the variations of the viscosity with time at the midpoint of the pipe for $n = 0.8$ and 0.6. The type of non-Newtonian fluid and the mean velocity primarily dictates the variation of viscosity. As seen in Fig. 14, the viscosity is higher when the fluid flow accelerates or decelerates. It is customary that in 2D simulations, the viscosity is higher in the proximity of the pipe wall (Majd et al. 2016) because of higher variations of velocity in that region. Likewise, a large amount of change in velocity over time, which corresponds to significant variations in space, is analogous to the conditions in the region of the pipe wall neighborhood and can produce considerable viscosity. A similar trend is also observed for the variations of shear stress, as seen in Fig. 15.

Summary and Conclusions

The prediction of transient friction is an important concern, allowing for the estimation of the damping of pressure histories.

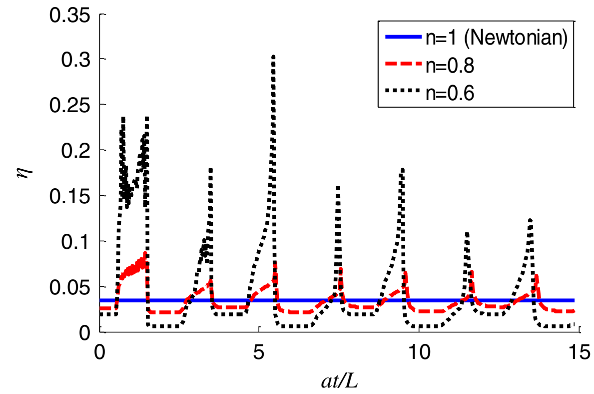

Fig. 14. Dynamic viscosity during the transient flow at the midpoint of the pipeline.

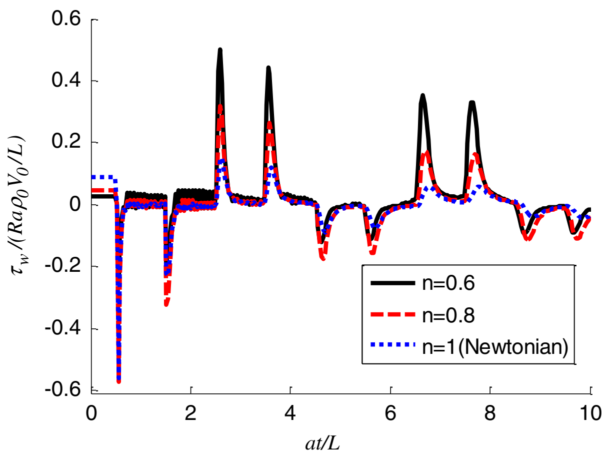

Fig. 15. Nondimensional wall shear stress at the midpoint of the pipeline.

For non-Newtonian fluids, the mathematical representation of the friction term in the momentum equation consists of the shear rate determined by the velocity profile at each cross section. As a result, at least a 2D formulation of transient flow is required that includes variations of velocity in the axial direction and also in the radial direction. The 2D methods are not efficient and appropriate for practical applications because they are computationally cumbersome. To overcome the difficulties associated with the calculation of the velocity profile, a 1D solution approach for non-Newtonian fluids is proposed in this research based on Zielke's model.

The Zielke model adopts a convolution integral of flow acceleration with weight functions to calculate the transient friction term. In this approach, the required cross-sectional velocity gradient of the power-law and Cross fluid in the transient state was computed according to that of the steady-state flow. This is equivalent to assuming the Hagen–Poiseuille velocity profile during the unsteady flow. On this basis, the appropriate governing equations were derived and were solved numerically using the MOC.

The proposed method did not consider the variations of the velocity profile, and hence, it approximated the shear rate, wall shear stress, and viscosity using the average velocity of flow. The derivation of the viscosity in terms of the mean velocity was performed for steady-state flow. Nevertheless, the viscosity was updated at each time step iteratively based on flow variations. For the sake of validation of the proposed method, the experimental and 2D results were compared. Both comparisons presented in terms of pressure head and mean velocity seemed reasonable.

The pressure histories of the non-Newtonian fluid hammer revealed significant changes compared to Newtonian fluids. The proposed 1D formulas and corresponding MOC solution, similar to the 2D models, could favorably capture the non-Newtonian effects. The maximum error between the proposed and the 2D model was less than two percent, which had a decreasing trend when the power-law index approaches one (non-Newtonian fluids).

Appendix I. Shear Stress in Power-Law Fluids

The purpose of this appendix is to study the fully developed steady flow in a pipe of radius R, as exhibited in Fig. 16. The steady flow is due to the pressure difference across the two ends of the pipe. Since there is no angular velocity and the flow is steady, the linear momentum balance (in the direction of flow, z) on a fluid element ABCD of radius r and length L, may be written as

$$p(\pi r^2) - (p + \Delta p)(\pi r^2) = \tau_{rz}(2\pi rL) \quad \text{or} \quad \tau_{rz} = \left(\frac{r}{2}\right)\left(-\frac{\Delta p}{L}\right) \tag{25}$$

This shows the linear variation of the shear stress across the pipe cross section, increasing from zero at the axis of the pipe to a maximum value at the wall of the pipe. It should be emphasized here that Eq. (25) is applicable to both laminar and turbulent flow of any incompressible fluid in steady, fully developed conditions since it is based simply on a force balance and no assumption has been made regarding either the type of fluid or the flow pattern. Eq. (25) thus provides a convenient basis for determining the shear stress at the wall of the pipe τ_w as

$$\tau_w = \left(\frac{R}{2}\right)\left(-\frac{\Delta p}{L}\right) \tag{26}$$

the shear stress may then be evaluated in terms of the shear rate at the wall, $\dot{\gamma}_w$ or $(-dV_z/dr)_w$ to yield steady shear stress–shear rate data for a fluid. This relationship may be obtained, however, because the z-component of the velocity is a function only of the radial coordinate, i.e., $V_z(r)$. The volumetric flow rate through the annulus formed by two concentric fluid elements at radial positions of r and $(r + dr)$, as shown in Fig. 16(b). The volumetric flow rate is given by

$$dQ = 2\pi V_z(r)dr \tag{27}$$

for the sake of simplicity, $V_z(r)$ will now be written as V_z. The total volumetric flow rate is obtained by integrating Eq. (27) over the cross section of the pipe as

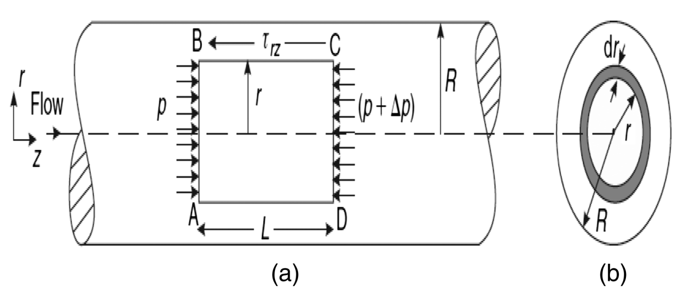

Fig. 16. Schematics of flow in a pipe. (Reprinted from *Non-Newtonian Flow and Applied Rheology*, R. P. Chhabra and J. F. Richardson, © 2008, with permission from Elsevier.)

$$Q = \int_0^R 2\pi r V_z dr \tag{28}$$

carrying out the integration in Eq. (28) by parts

$$Q = 2\pi\left\{\left(\frac{r^2}{2}V_z\right)\Big|_0^R + \int_0^R \frac{r^2}{2}\left(\frac{-dV_z}{dr}\right)dr\right\} \tag{29}$$

Considering the no-slip condition at the pipe wall, i.e., $V_z = 0$ at $r = R$, the first term on the right-hand side of Eq. (29) vanishes at both limits of integration. Therefore, Eq. (29) reduces to

$$Q = \pi \int_0^R r^2\left(\frac{-dV_z}{dr}\right)dr \tag{30}$$

For the laminar flow of time-independent fluids, the shear rate $(-dV_z/dr)$ is determined only by the value of the shear stress, i.e., the corresponding value of τ_{rz}. Thus, without any loss of generality, it is convenient to write this functional relationship as

$$\frac{-dV_z}{dr} = f(\tau_{rz}) \tag{31}$$

where f is a function dependent on the specified fluid description. The combination of Eqs. (25) and (26) yields

$$\frac{\tau_{rz}}{\tau_w} = \frac{r}{R} \tag{32}$$

or in terms of derivatives (for constant values of R and τ_w)

$$dr = \left(\frac{R}{\tau_w}\right)d\tau_{rz} \tag{33}$$

By substituting Eqs. (31) and (32) into Eq. (30), the discharge rate Q is provided as

$$Q = \frac{\pi R^3}{\tau_w^3}\int_0^{\tau_w} \tau_{rz}^2 f(\tau_{rz})d\tau_{rz} \tag{34}$$

in which, $f(\tau_{rz}) = \dot{\gamma}$. For instance, for a power-law model fluid

$$\tau_{rz} = m\left(\frac{-dV_z}{dr}\right)^n = m(\dot{\gamma})^n \tag{35}$$

therefore, the discharge rate Q Eq. (34) is obtained

$$Q = \frac{\pi R^3}{\tau_w^3}\int_0^{\tau_w} \tau_{rz}^2\left(\frac{\tau_{rz}}{m}\right)^{1/n} d\tau_{rz} \tag{36}$$

Appendix II. Relation between Shear Rate, Mean Velocity, and Shear Stress

The Eq. (34) is a general formulation relating the shear stress to the shear rate characteristics of a time-independent fluid dictated by the rheological data of a specified fluid. Eq. (34) is rearranged as:

$$\left(\frac{Q}{\pi R^3}\right)\tau_w^3 = \int_0^{\tau_w} \tau_{rz}^2 f(\tau_{rz})d\tau_{rz} \tag{37}$$

The right-hand side of Eq. (37) accounts for a definite integral; hence, the final result depends only on the value of the wall shear stress, τ_w, and not on the nature of the continuous function $f(\tau_{rz})$. As a consequence, one should only evaluate the wall shear stress τ_w [Eq. (26)] and the corresponding shear rate at the wall (dV_z/dr) at $r = R$, or simply $f(\tau_w)$. The Leibnitz rule allows for the derivative of a definite integral of the form $(d/ds')\{\int_0^{s'} s^2 f(s)ds\}$ to be written as $(s')^2 f(s')$, where s is a dummy variable of integration (τ_{rz} here) and s' is naturally identified as τ_w. Applying the Leibnitz rule to Eq. (37) when differentiated with respect to τ_w enables

$$\frac{d}{d\tau_w}\left\{\left(\frac{Q}{\pi R^3}\right)\tau_w^3\right\} = \frac{d}{d\tau_w}\left\{\int_0^{\tau_w} \tau_{rz}^2 f(\tau_{rz})d\tau_{rz}\right\}$$

which further simplification gives

$$(3\tau_w^2)\left(\frac{Q}{\pi R^3}\right) + \tau_w^3\frac{d}{d\tau_w}\left(\frac{Q}{\pi R^3}\right) = \tau_w^2 f(\tau_w) \tag{38}$$

Eq. (38) can be rearranged as

$$f(\tau_w) = 3\left(\frac{Q}{\pi R^3}\right) + \tau_w\frac{d}{d\tau_w}\left(\frac{Q}{\pi R^3}\right) \tag{39}$$

The use is made of the relation $d\ln x = x^{-1}dx$ so that Eq. (39) may be written as

$$f(\tau_w) = \left(-\frac{dV_z}{dr}\right)_w = \frac{4Q}{\pi R^3}\left\{\frac{3}{4} + \frac{1}{4}\frac{d\ln(\frac{4Q}{\pi R^3})}{d\ln(\tau_w)}\right\} \tag{40}$$

or, in terms of the mean velocity over the flow cross section, $Q = V\pi R^2$, and pipe diameter D

$$\left(-\frac{dV_z}{dr}\right)_w = \left(\frac{8V}{D}\right)\left\{\frac{3}{4} + \frac{1}{4}\frac{d\ln(\frac{8V}{D})}{d\ln\tau_w}\right\} \tag{41}$$

Eq. (41) may also be written as follows:

$$\dot{\gamma} = \left(\frac{8V}{D}\right)\left(\frac{3(d\ln\tau_w)(d\ln(8V/D))^{-1} + 1}{4(d\ln\tau_w)(d\ln(8V/D))^{-1}}\right) \tag{42}$$

Appendix III. Derivation of Coefficients of Characteristics Equations

The MOC allows for writing the momentum and continuity equations, as follows:

$$\mathrm{C}^+\colon \frac{dQ}{dt} + \frac{gA}{c}\frac{dH}{dt} + \frac{1}{2}A\Delta t\lambda\rho\frac{|Q_A|Q_P}{A^2} + \frac{16\upsilon}{D^2}\sum_{k=1}^{N} Y_k(t) = 0,$$

$$Y_k(t) = \sum_{k=1}^{N_{UF}} m_k \mathrm{e}^{-\frac{4\nu}{D^2}n_k t}\int_0^t \mathrm{e}^{\frac{4\nu}{D^2}n_k s}\frac{\partial V}{\partial s}(s)ds \tag{43}$$

$$\mathrm{C}^-\colon \frac{dQ}{dt} - \frac{gA}{c}\frac{dH}{dt} + \frac{1}{2}A\Delta t\lambda\rho\frac{|Q_B|Q_P}{A^2} + \frac{16\upsilon}{D^2}\sum_{k=1}^{N} Y_k(t) = 0,$$

$$Y_k(t) = \sum_{k=1}^{N_{UF}} m_k \mathrm{e}^{-\frac{4\nu}{D^2}n_k t}\int_0^t \mathrm{e}^{\frac{4\nu}{D^2}n_k s}\frac{\partial V}{\partial s}(s)ds \tag{44}$$

Here, Eq. (43) is valid on the path $dz/dt = a$, and Eq. (44) is valid on $dz/dt = -a$. Note that the last terms of these equations (unsteady friction terms) contain $\partial Q/\partial t$, which requires the discharge Q_P at the unknown time step $n+1$. The aim is to obtain algebraic relations to approximate H_P and Q_P unknowns at each time and space step (subscripts A and B stand for the left and the right node on the characteristic lines, respectively). Finite difference approximation of Eqs. (43) and (44) yields

$$C^{+}:Q_P - Q_A + \frac{gA}{a}(H_P - H_A) + \frac{1}{2}A\Delta t\lambda\rho\frac{|Q_A|Q_P}{A^2} + A\Delta t\frac{16\upsilon}{D^2}\sum_{k=1}^{N} Y_k(t) = 0 \tag{45}$$

$$C^{-}:Q_P - Q_B - \frac{gA}{a}(H_P - H_B) + \frac{1}{2}A\Delta t\lambda\rho\frac{|Q_B|Q_P}{A^2} + A\Delta t\frac{16\upsilon}{D^2}\sum_{k=1}^{N} Y_k(t) = 0 \tag{46}$$

Alternatively

$$C^{+}:Q_P - Q_A + \frac{gA}{a}(H_P - H_A) = -A\Delta t e_1, \qquad e_1 = \frac{1}{2}\lambda\rho\frac{|Q_A|Q_P}{A^2} + \frac{16\upsilon}{D^2}\sum_{k=1}^{N} Y_k(t), \qquad Y_k(t) = \sum_{k=1}^{N_{UF}} m_k e^{-\frac{4\upsilon}{D^2}n_k t}\int_0^t e^{\frac{4\upsilon}{D^2}n_k s}\frac{\partial V}{\partial s}(s)ds \tag{47}$$

and

$$C^{-}:Q_P - Q_B - \frac{gA}{a}(H_P - H_B) = -A\Delta t e_2, \qquad e_2 = \frac{1}{2}\lambda\rho\frac{|Q_B|Q_P}{A^2} + \frac{16\upsilon}{D^2}\sum_{k=1}^{N} Y_k(t), \qquad Y_k(t) = \sum_{k=1}^{N_{UF}} m_k e^{-\frac{4\upsilon}{D^2}n_k t}\int_0^t e^{\frac{4\upsilon}{D^2}n_k s}\frac{\partial V}{\partial s}(s)ds \tag{48}$$

where m_k, n_k = parameters of Trikha's (1975) or Vardy et al.'s (1993) unsteady friction formulation. The last term of these equations contains a convolution integral to be evaluated numerically. In fact, the term $Y(t)$ in Eqs. (47) and (48) is used to model unsteady friction. Considering the weighting function given by Eq. (7), the UF convolution integrals are computed by (Keramat and Tijsseling 2012)

$$Y_k(t) \coloneqq \int_0^t\left(\sum_{k=1}^{N_{UF}} m_k e^{-\frac{4\upsilon}{D^2}n_k(t-s)}\frac{\partial V}{\partial s}(s)\right)ds = \sum_{k=1}^{N_{UF}} m_k e^{-\frac{4\upsilon}{D^2}n_k t}\int_0^t e^{\frac{4\upsilon}{D^2}n_k s}\frac{\partial V}{\partial s}(s)ds \coloneqq \sum_{k=1}^{N_{UF}} Y_k(t) \tag{49}$$

The use of exponential weighting functions permits a recursive formula to evaluate the convolution integrals. To this aim, considering time step Δt, Y_k at the previous time step is

$$Y_k(t-\Delta t) = \int_0^{t-\Delta t} m_k e^{-\frac{4\upsilon n_k}{D^2}(t-\Delta t-s)}\frac{\partial V}{\partial s}(s)ds = e^{\frac{4\upsilon n_k}{D^2}\Delta t} m_k e^{-\frac{4\upsilon n_k}{D^2}t}\int_0^{t-\Delta t} e^{\frac{4\upsilon n_k}{D^2}s}\frac{\partial V}{\partial s}(s)ds \tag{50}$$

Accordingly, $Y(t)$ can be approximated as follows (Keramat and Tijsseling 2012):

$$\begin{aligned}
Y_k(t) &= \sum_{k=1}^{N_{UF}} Y_k(t) = \sum_{k=1}^{N_{UF}} m_k e^{-\frac{4\upsilon n_k}{D^2}t}\left(\int_0^{t-\Delta t} e^{\frac{4\upsilon n_k}{D^2}s}\frac{\partial V}{\partial s}(s)ds + \int_{t-\Delta t}^{t} e^{\frac{4\upsilon n_k}{D^2}s}\frac{\partial V}{\partial s}(s)ds\right)\\
&= \sum_{k=1}^{N_{UF}}\left(m_k e^{-\frac{4\upsilon n_k}{D^2}t}\int_0^{t-\Delta t} e^{\frac{4\upsilon n_k}{D^2}s}\frac{\partial V}{\partial s}(s)ds\right) + \sum_{k=1}^{N_{UF}}\left(m_k e^{-\frac{4\upsilon n_k}{D^2}t}\int_{t-\Delta t}^{t} e^{\frac{4\upsilon n_k}{D^2}s}\frac{\partial V}{\partial s}(s)ds\right)\\
&= \sum_{k=1}^{N_{UF}}\left(m_k e^{-\frac{4\upsilon n_k}{D^2}t}\int_0^{t-\Delta t} e^{\frac{4\upsilon n_k}{D^2}s}\frac{\partial V}{\partial s}(s)ds\right) + \sum_{k=1}^{N_{UF}}\left(m_k e^{-\frac{4\upsilon n_k}{D^2}t}\int_{t-\Delta t}^{t} e^{\frac{4\upsilon n_k}{D^2}s}\frac{\partial V}{\partial s}(s)ds\right)\\
&\approx \sum_{k=1}^{N_{UF}} e^{-\frac{4\upsilon n_k}{D^2}\Delta t} Y_k(t-\Delta t) + \sum_{k=1}^{N_{UF}} m_k e^{-\frac{4\upsilon n_k}{D^2}t} e^{\frac{4\upsilon n_k}{D^2}t}([V(t)] - [V(t-\Delta t)])\\
&= \left(\sum_{k=1}^{N_{UF}} m_k\right)[V(t)] + \sum_{k=1}^{N_{UF}}\left\{e^{-\frac{4\upsilon n_k}{D^2}\Delta t} Y_k(t-\Delta t) - m_k[V(t-\Delta t)]\right\}\\
&= \frac{Q_P}{A}\left(\sum_{k=1}^{N_{UF}} m_k\right) + \sum_{k=1}^{N_{UF}}\left\{e^{-\frac{4\upsilon n_k}{D^2}\Delta t} Y_k(t-\Delta t) - \frac{m_k}{A}[Q(t-\Delta t)]\right\}
\end{aligned} \tag{51}$$

the result of Eq. (51) is substituted in Eq. (47) for C^{+}

$$e_1 = \lambda\rho\frac{|Q_A|Q_P}{2A^2} + \frac{16\upsilon}{D^2}\sum_{k=1}^{N_{UF}}\left\{e^{-\frac{4\upsilon\Delta t}{D^2}n_k} Y_k(t-\Delta t) - \frac{m_k}{A}[Q(t-\Delta t)]\right\} + \frac{16\upsilon}{AD^2}\left(\sum_{k=1}^{N_{UF}} m_k\right)Q_P \tag{52}$$

In power-law fluids, kinematic viscosity (υ) in Eq. (52) depends on the velocity gradient (dV/dr). Considering Eq. (11), kinematic viscosity (υ) may be written as

$$\upsilon = \frac{\mu}{\rho} = \frac{1}{\rho}m\left(\frac{dV}{dr}\right)^{n-1} = \underbrace{\frac{1}{\rho}m\left(\left(\frac{3n+1}{4n}\right)\left(\frac{8}{AD}\right)\right)^{n-1}}_{L_1} Q_P^{n-1} = L_1 Q_P^{n-1} \tag{53}$$

in which, m = power-law consistency coefficient, and n = power-law index. By substituting Eq. (53) in Eq. (52) and after some simplifications, the following relation is obtained:

$$e_1 = e_3 Q_{P,r+1} + e_4 + e_5 Q_{P,r+1} \tag{54}$$

$$e_3 = \lambda\rho \frac{|Q_A|}{2A^2},$$

$$e_4 = \frac{16L_1(Q_{P,r}^{n-1})}{D^2} \sum_{k=1}^{N_{UF}} \left\{ \mathrm{e}^{-\frac{4L_1(Q_{P,r}^{n-1})\Delta t}{D^2} n_k} Y_k(t-\Delta t) - \frac{m_k}{A}[Q(t-\Delta t)] \right\},$$

$$e_5 = \frac{16L_1(Q_{P,r}^{n-1})}{AD^2} \sum_{k=1}^{N_{UF}} m_k \tag{55}$$

in which subscript r = different iterations and $Q_{P,r}$ for $r = 1$ adapts $Q(t-\Delta t)$. Substitution of Eq. (54) in Eq. (47) yields the updated Q_P from C^+ (subscript $r + 1$ stands for the updated quantities)

$$Q_{P,r+1} = Q_A - \frac{gA}{a} H_{P,r+1} + \frac{gA}{a} H_A - A\Delta t e_3 Q_{P,r+1} - A\Delta t e_4 - A\Delta t e_5 Q_{P,r+1} \tag{56}$$

or

$$Q_{P,r+1} = -\frac{B}{1 + C'_{P2} + C''_{P2}} H_{P,r+1} + \frac{Q_A + BH_A + C'_{P1} + C''_{P1}}{1 + C'_{P2} + C''_{P2}} \tag{57}$$

So that

$$C^+ : Q_{P,r+1} = C_P - C_{a+} H_{P,r+1}, \quad C_P = \frac{Q_A + BH_A + C'_{P1} + C''_{P1}}{1 + C'_{P2} + C''_{P2}}, \quad C_{a+} = \frac{B}{1 + C'_{P2} + C''_{P2}} \tag{58}$$

Likewise, for the C^- characteristics equation, we have

$$C^- : Q_{P,r+1} = C_N + C_{a-} H_{P,r+1}, \quad C_N = \frac{Q_B - BH_B + C'_{N1} + C''_{N1}}{1 + C'_{N2} + C''_{N2}}, \quad C_{a-} = \frac{B}{1 + C'_{N2} + C''_{N2}} \tag{59}$$

The coefficients holding superscripts ′ and ″ refer to the steady-state friction and the unsteady friction, respectively. The numerical descriptions of each coefficient are presented in Table 1.

Table 1. Coefficients C_{P1}, C_{P2}, C_{N1}, and C_{N2}

Analysis type	$C'_{P1}, C'_{P2}, C''_{P1}, C''_{P2}$	$C'_{N1}, C'_{N2}, C''_{N1}, C''_{N2}$
Steady-state friction [′]		
Frictionless	$C'_{P1} = C'_{P2} = 0$	$C'_{N1} = C'_{N2} = 0$
First-order accuracy	$C'_{P1} = -R\Delta t\|Q_A\|Q_A$	$C'_{N1} = -R\Delta t\|Q_B\|Q_B$
	$C'_{P2} = 0$	$C'_{N2} = 0$
Second-order accuracy	$C'_{P1} = 0$	$C'_{N1} = 0$
	$C'_{P2} = R\Delta t\|Q_A\|$	$C'_{N2} = R\Delta t\|Q_B\|$
	$R = \frac{1}{2}\frac{\lambda\rho}{A}, B = \frac{gA}{a}$	
Unsteady friction [″]		
No-unsteady friction and non-Newtonian	$C''_{P1} = 0$	$C''_{N1} = 0$
	$C''_{P2} = 0$	$C''_{N2} = 0$
Unsteady friction and non-Newtonian	$C''_{P1} = -A\Delta t e_4$	$C''_{N1} = -A\Delta t e_4$
	$C''_{P2} = A\Delta t e_5$	$C''_{N2} = A\Delta t e_5$

Data Availability Statement

All data, models, or code generated or used during the study are available from the corresponding author by request.

Notation

The following symbols are used in this paper:

A = pipe's internal cross-sectional area;
a = elastic wave speed;
C^* = Vardy and Brown's (1995) shear decay coefficient;
D = pipe diameter;
g = gravitational acceleration;
H = piezometric head;
k, n = two fitting parameters (Cross model);
L = pipe length;
m = power-law consistency coefficient;
m_k, n_k = parameters of Trikha's (1975) or Vardy et al.'s (1993) unsteady friction formulation;
n = power-law index;
Q = discharge rate;
$\mathbf{R}$ = Reynolds number;
R = pipe radius;
r = distance in the radial direction from the pipe axis;
t = time;
u = axial component of velocity;
V = average cross-sectional velocity;
V_z = axial (z-component) velocity;
V_0 = initial velocity;
W = weighting function;
z = distance along the pipe centerline;
β_s = quasi-steady friction;
β_u = unsteady friction;
$\dot{\gamma}$ = Shear rate;
Δt = time step;
Δz = space-step increment;
η = dynamic viscosity of non-Newtonian fluid;
η_0 = limiting values of the apparent viscosity at low shear rates;
η_∞ = limiting values of the apparent viscosity high shear rates;
λ = Darcy–Weisbach friction coefficient;
μ = dynamic viscosity of the Newtonian fluid;
υ = kinematic viscosity;
τ_{rz} = shear stress point value;
τ_w = shear stress at the wall;
$\tau_{w,ss}$ = quasi-steady shear stress at the wall; and
ρ = fluid density.

References

Achard, L., and G. M. Lespinard. 1981. "Structure of the transient wall-law in one-dimensional models of laminar pipe flows." *J. Fluid Mech.* 113: 283–298. https://doi.org/10.1017/S0022112081003509.

Azhdari, M., A. Riasi, and P. Tazraei. 2017. "Numerical study of non-Newtonian effects on fast transient flows in helical pipes." Preprint, submitted March 19, 2017. https://arxiv.org/abs/1703.06877.

Bird, R. B., R. C. Armstrong, and O. Hassager. 1987. Vol. 1 of *Dynamics of polymeric liquids*. 2nd ed. New York: Wiley.

Brown, E. T. 1984. "On weighting functions for the simulation of unsteady turbulent flow." In *Forum on unsteady flow*, 26–28. New York: ASME.

Brunone, B., U. M. Golia, and M. Greco. 1991. "Some remarks on the momentum equation for fast transients." In *Proc., Int. Meeting on Hydraulic Transients and Water Column Separation*, edited by E. Cabrera and M. A. Fanelli, 201–209. Valencia, Spain: Universitat Politècnica de València.

Brunone, B., U. M. Golia, and M. Greco. 1995. "The effects of two-dimensionality on pipe transients modeling." *J. Hydraul. Eng.* 121 (12): 906–912. https://doi.org/10.1061/(ASCE)0733-9429(1995)121:12(906).

Brunone, B., B. W. Karney, M. Mecarelli, and M. Ferrante. 2000. "Velocity profiles and unsteady pipe friction in transient flow." *J. Water Resour. Plann. Manage.* 126 (4): 236–244. https://doi.org/10.1061/(ASCE)0733-9496(2000)126:4(236).

Chaudhry, M. H. 2014. *Applied hydraulic transients*. 3rd ed. New York: Springer.

Chen, Z., and R. Barbieri. 2013. "Engineering approaches to study cardiovascular physiology: Modeling, estimation, and signal processing." *J. Front. Physiol.* 3 (378): 1–135. https://doi.org/10.3389/fphys.2012.00425.

Chhabra, R. P., and J. F. Richardson. 2011. *Non-Newtonian flow and applied rheology: Engineering applications*. 2nd ed. Amsterdam, Netherlands: Elsevier Science.

Daily, J. W., W. L. Hankey, R. W. Olive, and J. M. Jordaan. 1956. "Resistance coefficients for accelerated and decelerated flows through smooth tubes and orifices." *Trans. ASME* 78: 1071–1077.

Dodge, D. W., and A. B. Metzner. 1959. "Turbulent flow of non-Newtonian systems." *J. AIChE* 5 (2): 189–204. https://doi.org/10.1002/aic.690050214.

Escudier, M. P., D. M. Jones, and I. Gouldson. 1992. "Fully developed flow of shear-thinning fluids." In *Proc. 6th Int. Symp. on Applied Laser Techniques to Fluid Mechanics*. Berlin: Springer.

Ghidaoui, M. S., and S. Mansour. 2002. "Efficient treatment of the Vardy-Brown unsteady shear in pipe transients." *J. Hydraul. Eng.* 128 (1): 102–112. https://doi.org/10.1061/(ASCE)0733-9429(2002)128:1(102).

He, Q., J. Huang, X. Shi, X. P. Wang, and C. Bi. 2016. "Numerical simulation of 2D unsteady shear-thinning non-Newtonian incompressible fluid in screw extruder with fictitious domain method." *J. Comput. Math. Appl.* 73 (1): 109–121. https://doi.org/10.1016/j.camwa.2016.11.005.

Holmboe, E. L., and W. T. Rouleau. 1967. "The effect of viscous shear on transients in liquid lines." *J. Basic Eng.* 89 (1): 174–180. https://doi.org/10.1115/1.3609549.

Ikoku, C. U., and H. J. Ramey Jr. 1978. "Transient flow of non-Newtonian power-law fluids in porous media." *J. Soc. Petrol. Eng.* 19 (3): 164–174. https://doi.org/10.2118/7139-PA.

Irgens, F. 2013. *Rheology and non-Newtonian fluids*. New York: Springer.

Kagawa, T., I. Lee, A. Kitagawa, and T. Takenaka. 1983. "High speed and accurate computing method of frequency-dependent friction in laminar pipe flow for characteristics method." *Trans. JSME* 49 (447): 2638–2644. https://doi.org/10.1299/kikaib.49.2638.

Keramat, A., and A. S. Tijsseling. 2012. "Waterhammer with column separation, fluid-structure interaction and unsteady friction in a viscoelastic pipe." In *Centre for analysis, scientific computing and applications*. Eindhoven, Netherlands: Dept. of Mathematics and Computer Science, Eindhoven Univ. of Technology.

Khan, M. M. K. 1992. "Friction factor and flow characterisation of non-Newtonian fluids." In *Proc., 11th Australian Fluid Mechanics Conf.*, 1029–1031. Hobart, TAS: Univ. of Tasmania.

Majd, A., A. Ahmadi, and A. Keramat. 2016. "Investigation of non-Newtonian fluid effects during transient flows in a pipeline." *J. Mech. Eng.* 62 (2): 105–115. https://doi.org/10.5545/sv-jme.2015.2787.

Martins, N. C., B. Brunone, S. Meniconi, H. M. Ramos, and I. D. Covas. 2018. "Efficient CFD model for transient laminar flow modeling: Pressure wave propagation and velocity profile changes." *J. Fluids Eng.* 140 (1): 011102. https://doi.org/10.1115/1.4037504.

Metzner, A. B., and J. C. Reed. 1955. "Flow of non-Newtonian fluids–correlation of the laminar, transition, and turbulent flow regions." *J. AIChE* 1 (4): 434–440. https://doi.org/10.1002/aic.690010409.

Pezzinga, G. 1999. "Quasi-2D model for unsteady flow in pipe networks." *J. Hydraul. Eng.* 125 (7): 676–685. https://doi.org/10.1061/(ASCE)0733-9429(1999)125:7(676).

Pezzinga, G. 2000. "Evaluation of unsteady flow resistances by quasi-2D or 1D models." *J. Hydraul. Eng.* 126 (10): 778–785. https://doi.org/10.1061/(ASCE)0733-9429(2000)126:10(778).

Pezzinga, G., B. Brunone, D. Cannizzaro, M. Ferrante, S. Meniconi, and A. Berni. 2014. "Two-dimensional features of viscoelastic models of pipe transients." *J. Hydraul. Eng.* 140 (8): 04014036. https://doi.org/10.1061/(ASCE)HY.1943-7900.0000891.

Pinho, F. T., and J. H. Whitelaw. 1990. "Flow of non-Newtonian fluids in a pipe." *J. Non-Newtonian Fluid Mech.* 34 (2): 129–144. https://doi.org/10.1016/0377-0257(90)80015-R.

Sadikin, A., M. K. Bahrin, A. Ismail, S. Ahmad, S. M. Salleh, M. N. Abdol Rahman, A. Sapit, and S. S. Ayop. 2018. "Numerical simulation in transient flow of non-Newtonian fluid in nozzles during filling process." *Int. J. Integr. Eng.* 10 (1): 92–95. https://doi.org/10.30880/ijie.2018.10.01.014.

Suzuki, K., T. Taketomi, and S. Sato. 1991. "Improving Zielke's method of simulating frequency-dependent friction in laminar liquid pipe flow." *J. Fluids Eng.* 113 (4): 569–573. https://doi.org/10.1115/1.2926516.

Tazraei, P., and A. Riasi. 2015. "Quasi-two-dimensional numerical analysis of fast transient flows considering non-Newtonian effects." *J. Fluids Eng.* 138 (1): 1–8. https://doi.org/10.1115/1.4031093.

Toms, B. A. 1948. "Some observation on the flow of linear polymer solutions through straight tubes at large {R}eynolds numbers." In *Proc. 1st Int. Congress on Rheology*. Washington, DC: Allen Institute for Artificial Intelligence.

Travaš, V., and S. Basara. 2015. "A mixed MOC/FDM numerical formulation for hydraulic transients." *Tech. Gaz.* 22 (5): 1141–1147. https://doi.org/10.17559/TV-20131004142635.

Trikha, A. K. 1975. "An efficient method for simulating frequency-dependent friction in transient liquid flow." *J. Hydraul. Eng.* 97 (1): 97–105. https://doi.org/10.1115/1.3447224.

Vardy, A. E., and J. M. B. Brown. 1995. "Transient, turbulent, smooth pipe friction." *J. Hydraul. Res.* 33 (4): 435–456. https://doi.org/10.1080/00221689509498654.

Vardy, A. E., and J. M. B. Brown. 1996. "On turbulent, unsteady, smooth-pipe flow." In *Proc., Int. Conf. on Pressure Surges and Fluid Transients*, 289–311. Harrogate, UK: BHR Group.

Vardy, A. E., and J. M. B. Brown. 2003. "Transient turbulent friction in smooth pipe flows." *J. Sound Vibr.* 259 (5): 1011–1036. https://doi.org/10.1006/jsvi.2002.5160.

Vardy, A. E., and J. M. B. Brown. 2004a. "Efficient approximation of unsteady friction weighting functions." *J. Hydraul. Eng.* 130 (11): 1097–1107. https://doi.org/10.1061/(ASCE)0733-9429(2004)130:11(1097).

Vardy, A. E., and J. M. B. Brown. 2004b. "Transient turbulent friction in fully rough pipe flows." *J. Sound Vib.* 270 (1–2): 233–257. https://doi.org/10.1016/S0022-460X(03)00492-9.

Vardy, A. E., and J. M. B. Brown. 2010. "Influence of time-dependent viscosity on wall shear stresses in unsteady pipe flows." *J. Hydraul. Res.* 48 (2): 225–237. https://doi.org/10.1080/00221681003726221.

Vardy, A. E., and J. M. B. Brown. 2011. "Laminar pipe flow with time-dependent viscosity." *J. Hydroinf.* 13 (4): 729–740. https://doi.org/10.2166/hydro.2010.073.

Vardy, A. E., and K.-L. Hwang. 1991. "A characteristics model of transient friction in pipes." *J. Hydraul. Res.* 29 (5): 669–684. https://doi.org/10.1080/00221689109498983.

Vardy, A. E., K.-L. Hwang, and J. Brown. 1993. "A weighting function model of transient turbulent pipe friction." *J. Hydraul. Res.* 31 (4): 533–548. https://doi.org/10.1080/00221689309498876.

Vítkovský, J., M. Stephens, A. Bergant, L. Martin, and A. Simpson. 2004. "Efficient and accurate calculation of Zielke and Vardy-Brown unsteady friction in pipe transients." In *Proc., 9th Int. Conf. on Pressure Surges*, 405–419. Cranfield, UK: BHR Group.

Vítkovský, J., M. Stephens, A. Bergant, A. R. Simpson, and M. Lambert. 2006a. "Numerical error in weighting function-based unsteady friction model for pipe transients." *J. Hydraul. Eng.* 132 (7): 709–721. https://doi.org/10.1061/(ASCE)0733-9429(2006)132:7(709).

Vítkovský, J. P., A. Bergant, A. R. Simpson, and M. F. Lambert. 2006b. "Systematic evaluation of one-dimensional unsteady friction models in simple pipelines." *J. Hydraul. Eng.* 132 (7): 696–708. https://doi.org/10.1061/(ASCE)0733-9429(2006)132:7(696).

Wahba, E. M. 2006. "Runge–Kutta time-stepping schemes with TVD central differencing for the water hammer equations." *Int. J. Numer. Method Fluids* 52 (5): 571–590. https://doi.org/10.1002/fld.1188.

Wahba, E. M. 2013. "Non-Newtonian fluid hammer in elastic circular pipes: Shear-thinning and shear-thickening effects." *J. Non-Newtonian Fluid Mech.* 198 (Aug): 24–30. https://doi.org/10.1016/j.jnnfm.2013.04.007.

Wylie, E. B., V. L. Streeter, and L. Suo. 1993. *Fluid transients in systems*. Englewood Cliffs, NJ: Prentice Hall.

Zielke, W. 1968. "Frequency-dependent friction in transient pipe flow." *J. Basic Eng. Trans.* 90 (1): 109–115. https://doi.org/10.1115/1.3605049.